

Compressive behavior of concrete under high strain rates after freeze-thaw cycles

Xudong Chen^{*1}, Chen Chen^{1a}, Zhiheng Liu^{1b}, Jun Lu^{2c} and Xiangqian Fan^{2d}

¹College of Civil and Transportation Engineering, Hohai University, Nanjing, 210098, China

²Department of Materials and Structural Engineering, Nanjing Hydraulic Research Institute, Nanjing, 210024, China

(Received June 16, 2017, Revised November 6, 2017, Accepted November 7, 2017)

Abstract. The dynamic compressive behavior of concrete after freezing and thawing tests are investigated by using the split Hopkinson pressure bar (SHPB) technique. The stress-strain curves of concrete under dynamic loading are measured and analyzed. The setting numbers of freeze-thaw cycles are 0, 25, 50, and 75 cycles. Test results show that the dynamic strength decreases and peak strain increases with the increasing of freeze-thaw cycles. Based on the Weibull distribution model, statistical damage constitutive model for dynamic stress-strain response of concrete after freeze-thaw cycles was proposed. At last, the fragmentation test of concrete subjected to dynamic loading and freeze-thaw cycles is carried out using sieving statistics. The distributions of the fragment sizes are analyzed based on fractal theory. The fractal dimensions of concrete increase with the increasing of both freeze-thaw cycle and strain rate. The relations among the fractal dimension, strain rates and freeze-thawing cycles are developed.

Keywords: concrete; dynamic compressive behavior; freeze-thaw; fractal theory; strain rate

1. Introduction

Concrete pavements represent a large portion of the transportation infrastructure. Whereas many of these pavements provide excellent long-term performance, a portion of these pavements have recently shown premature joint deterioration (Li *et al.* 2012). During field inspections it has been observed that where the joints are damaged the sealant is damaged and the joint contained standing water. Research is needed to better understand how this standing water lead to freeze-thaw damage (Li *et al.* 2012).

Concrete subjected to repeated freeze-thaw cycles may deteriorate rapidly, or it may remain in service for many years without showing signs of distress (Lai *et al.* 2009, Lai *et al.* 2008, Safiuddin *et al.* 2014). Failure of the material may take the form of loss of strength, crumbling, or some combination of the two (Sun *et al.* 1999, Yun and Wu 2011, Shang *et al.* 2015). Concrete in a wet environment-in bridge piers, for example, pavement near oceans, wharves, and offshore structures, is especially vulnerable to freeze-thaw cycles (Choi and Yun 2014, Li *et al.* 2012).

Previous researches have been carried out on the durability of concrete with regard to the chemical aspects of concrete durability, resistance to freezing and thawing, and corrosion of reinforcing steel (Sun *et al.* 2002, Jiang *et al.* 2014, Tanyildizi 2017, Richard *et al.* 2016). Investigations on the effect of freezing and thawing on properties of concrete have focused on relative dynamic modulus, volume change, compressive strength, capillary absorption, and porosity of concrete (Richardson and Cushner 2015, AiTcin 2003, Lu *et al.* 2016). However, very little information is available on the freeze-thaw effect on dynamic mechanical properties of concrete (Chen and Qiao 2015).

When concrete is loaded dynamically, it has higher compressive and tensile strengths than that is loaded statically. Both tensile and compressive strengths of concrete increase with the strain rate and a critical strain rate exists beyond which large increases in strength occur (Xiao *et al.* 2015, Zhang *et al.* 2014, Daghast *et al.* 2016). Experimental data comes from tests performed on a variety of specimen sizes and by different techniques (Ozbolt *et al.* 2014, Lim *et al.* 2016). Different methods have been used to deliver the dynamic strength, the predominant of which is the split-Hopkinson pressure bar (SHPB) techniques (Chen *et al.* 2014, Tian *et al.* 2016). By using the SHPB technique, the impact behaviors of recycled aggregate concrete have been studied by Li *et al.* (2016, 2017).

Compressive behavior of plain concrete subjected to dynamic loading after various numbers of freeze-thaw cycles is investigated by using split Hopkinson pressure bar. The dynamic mechanical behavior of concrete was examined in terms of stress-strain curves, dynamic compressive strength and elastic modulus. In addition, a statistical damage constitutive model for compressive behavior of concrete after freeze-thaw tests was proposed.

*Corresponding author, Professor

E-mail: cxdong1985@163.com

^aPh.D. Student

E-mail: cxdong1985@163.com

^bUndergraduate Student

E-mail: 405471211@qq.com

^cSenior Engineer

E-mail: newlynewman1981@126.com

^dSenior Engineer

E-mail: xqfan@nhri.cn

Table 1 Mix proportion for concrete

| Concrete composition | Proportion (kg/m ³) |
|-----------------------|---------------------------------|
| Water | 180 |
| Cement | 380 |
| Sand | 668 |
| Coarse aggregate | 1089 |
| Fly ash | 94 |
| Superplasticizer | 4.75 |
| Water to binder ratio | 0.38 |

2. Experimental program

2.1 Specimen preparation

Cylindrical concrete specimens are tested in this experiment. The used cementitious material is ordinary 42.5 Portland cement and grade I fly ash according to Chinese standard. The river sand with a continuous grading from 0.4 to 2.5 mm is used. The coarse aggregate is crushed gravel with a maximum size of 10 mm. To obtain good flowability of the fresh mixture, 1.0 % mass fraction of polycarboxylate superplasticizer is added. The proportions of the mixture are shown in Table 1. The specimens are fabricated in polyvinyl chloride (PVC) molds.

The forms were removed after casting for 48 hours. Then, the specimens are cured in saturated calcium hydroxide solution for 180 days. Specimens are carefully cut at two ends by double-knife cut machine. For dynamic compressive testing, the specimens cylinders with the diameter of 74 mm and the height of 500 mm. The 16 cylindrical specimens with the diameter of 74 mm and the height of 148 mm are prepared for static compressive test. The average static compressive strength is 22.21 MPa.

2.2 Test procedures for freezing and thawing

The tests on concrete specimens are in accordance with ASTM C666 (2015). A single freeze-thaw cabinet was designed containing sixteen specimens was used. Seven freezing and thawing cycles on concrete specimens were cycled per day. A fundamental transverse frequency (FTF) of concrete was tested in accordance with ASTM C215

(2014) after each interval of nominally twenty-five freezing and thawing cycles and the surface-dried specimens were weighed. A spectrum analyzer equipped with transducers and a multi-counter was used to excite the specimens to vibrate, scan the frequency range of the vibrational response of the specimens and resolve the primary peak frequencies. Length change measurements were not taken since the aggregate were batched in the air-dry condition and meaningful expansion data were not anticipated. The values of the static compression strength after freeze-thaw cycles of 25, 50 and 100 are 18.55MPa, 14.53 MPa and 7.21 MPa, respectively.

2.3 Split Hopkinson pressure bar (SHPB) testing

The split Hopkinson pressure bar equipment at Hohai University's Cement and Concrete Research Lab features an input and output bar, each 3200mm and 1800mm long and 74mm in diameter, as shown in Fig. 1. They are made of 1045S steel, which carries a minimum strength of 630 MPa and a yield stress of 530 MPa. The striker bar is 37 mm in diameter and 600 mm in length. The striker is fired using compressed nitrogen gas. Both the input bar and output bar have two strain gages attached at mid-span. Detailed description for the SHPB testing of concrete specimens have been reviewed by Chen *et al.* (2013, 2014, 2015). The schematic diagram of the SHPB test setup is shown in Fig. 1.

3. Experimental results and discussion

3.1 Relative dynamic modulus (RDM) and mass loss

With the increasing of freeze-thaw cycles, the damage on the specimen can be observed. First, the originally smooth surface gradually became rough and fine aggregate was exposed. Portion of the surface peeled off from the skin until the entire specimen surface crisped off. Finally the coarse aggregate was exposed and some angularity fell. In the uniaxial compression test, along with the progress of the test, the specimen had undergone the stages of elastic deformation, cracks appearance, cracks development and destruction. The broken specimen was sectioned and it was found that the destruction was distributed inside the cement and along the transition zone between cement paste and

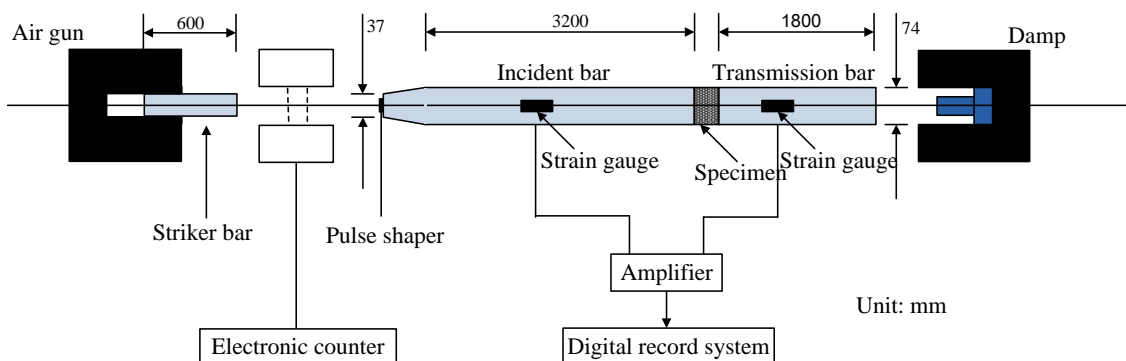


Fig. 1 The schematic diagram of the SHPB test setup

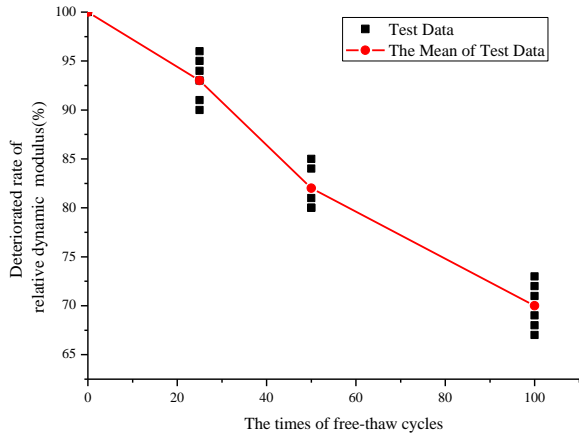


Fig. 2 The relationship between RDM (Relative Dynamic Modulus) and the freeze-thaw cycles

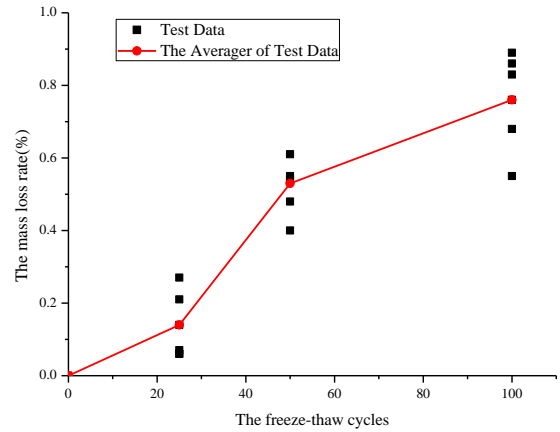


Fig. 3 The relationship between mass loss and the freeze-thaw cycles

aggregate. The coarse aggregate itself was not destroyed.

With the increase of freeze-thaw cycles the weight loss ratio and the loss ratio of the relative dynamic elastic modulus are increased. This phenomenon characterizes the development process of internal concrete structure damage deterioration. When the number of freeze-thaw cycles $N=0, 25, 50, 100$, the values of relative dynamic elastic modulus loss and mass loss are shown in Figs. 2 and 3.

As shown in Fig. 2, when the number of freeze-thaw cycles is less than 50, the mass loss of concrete increases slightly with the increasing of freeze-thaw cycles. This is because the cement mortar at the specimen surface crisped off slightly and the internal cracks did not develop. When the freeze-thaw cycles are in the range of 50 to 100, the growth of the mass loss is small and the mass loss versus cycles curve is more stable. This can be ascribed to the

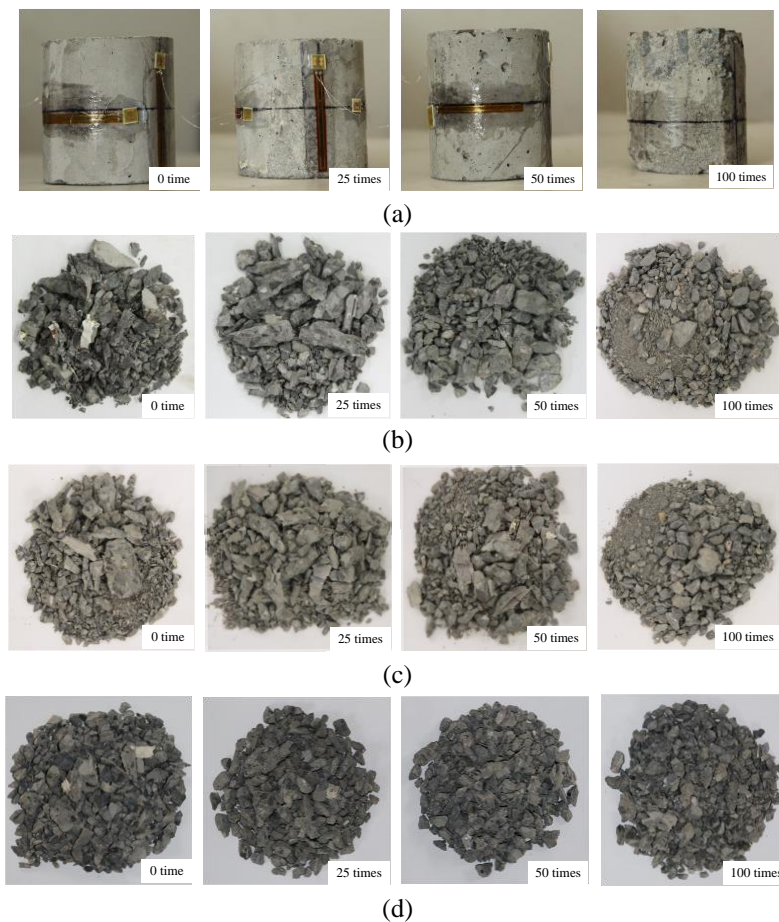


Fig. 4 The failure of specimen under different impact velocity: (a) $V=0$ m/s; (b) $V=8.52$ m/s; (c) $V=11.52$ m/s; (d) $V=13.56$ m/s

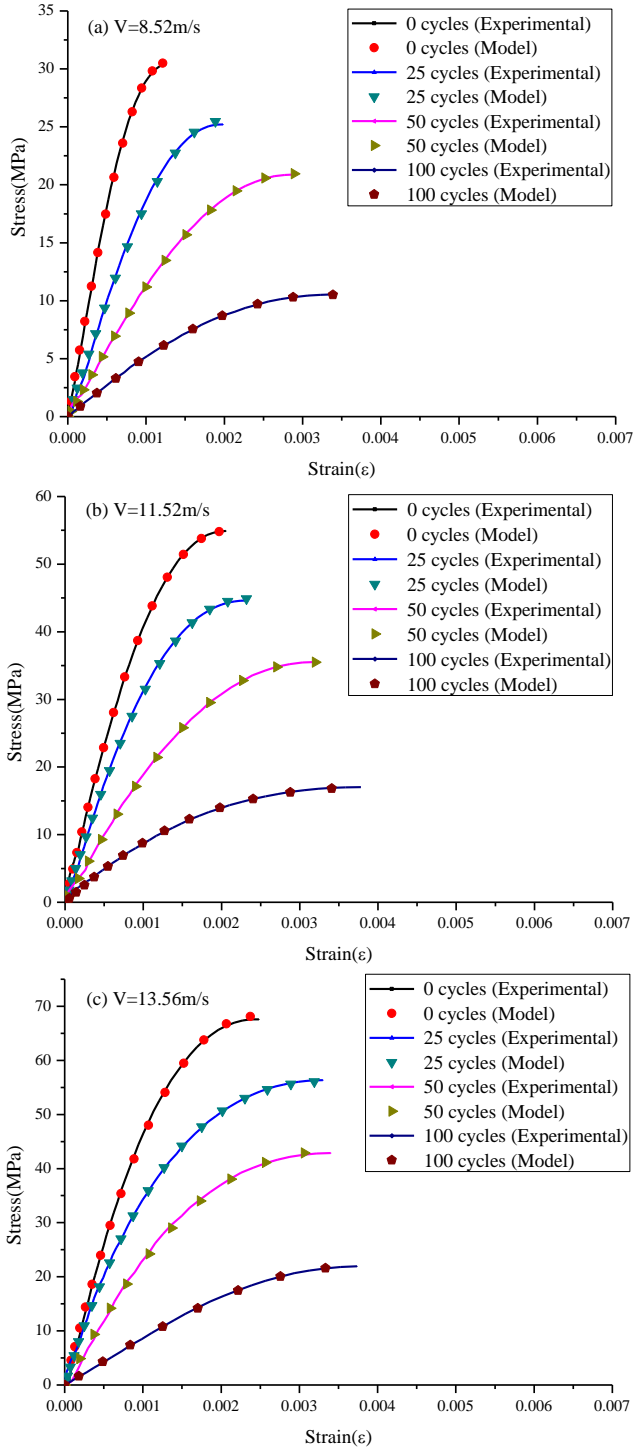


Fig. 5 The comparison between predicted and tested dynamic stress-strain relationships: (a) $V=8.52$ m/s; (b) $V=11.52$ m/s; (c) $V=13.56$ m/s

volume increasing in concrete caused by peeling off of the specimen surface and the absorbed water in internal micro cracks with the increasing of freeze-thaw cycles. Both of the two reasons interacted and thereby the curve shows relatively stable.

As shown in Fig. 3, when the freeze-thaw cycles are small, the relative dynamic elastic modulus of the concrete reduces very slowly and without noticeable damage. With

Table 2 The peak strain and compressive strength of concrete under different freeze-thaw cycles and impact velocities

| Impact velocity (m/s) | Freeze-thaw cycles | The peak strain | Compressive strength (MPa) |
|-----------------------|--------------------|-----------------|----------------------------|
| 8.52 | 0 | 0.001257 | 30.4013 |
| | 25 | 0.001983 | 25.1901 |
| | 50 | 0.002891 | 20.8834 |
| | 100 | 0.003387 | 10.5357 |
| 11.52 | 0 | 0.002057 | 54.8932 |
| | 25 | 0.002319 | 44.6125 |
| | 50 | 0.003197 | 35.5471 |
| | 100 | 0.003781 | 17.0407 |
| 13.56 | 0 | 0.002483 | 67.583 |
| | 25 | 0.003301 | 56.358 |
| | 50 | 0.003403 | 42.585 |
| | 100 | 0.003735 | 21.9315 |

the increasing of freeze-thaw cycles, the relative dynamic modulus downward trend is outstanding.

Also with the increase of the freeze-thaw cycles, the internal damage of concrete specimen is larger, so the axial compressive strength decreases with increasing of the freeze-thaw cycles.

3.2 The result of dynamic SHPB test

Fig. 4 shows the failure of specimen with different impact velocities and the cycles of freeze-thaw. With the increasing of the impact velocity and the numbers of freeze-thaw cycle, the failure of specimen is obvious.

When the peak strain of concrete is determined, the stress-strain curve of concrete before peak load can be obtained, as shown in Fig. 5. In Table 2, it can be found that the peak stress increased with the increasing of impact velocity while decreased with the increasing of the freeze-thaw cycles. The peak strain increased with the increasing of impact velocity and the freeze-thaw cycles.

3.3 Statistical damage model for concrete

The strength of concrete after freeze-thaw cycles decrease with the increasing of the freeze-thaw cycles. The reason can be attributed to the irreversible expansion of internal microcracks during freeze-thaw cycles, which leads to the irreversible superposition of damage and the decrease of the strength and durability. Here, the damage of concrete in freezing and thawing process can be written as

$$D_N = 0.006783N \quad (1)$$

where D_N is the concrete cumulative damage during freezing and thawing process with value of 0 to 1. When the freeze-thaw cycles is zero, the value of D_N is zero. N is the number of freeze-thaw cycles.

The static compressive strength of the concrete after freeze-thaw cycles can be expressed as (Liu and Wang 2012)

$$\sigma_c = \sigma_{c0}(1 - D_N) \quad (2)$$

where σ_c is the static compressive strength of the concrete after freeze-thaw, σ_{c0} is the compressive strength of concrete before freeze-thaw.

For material like-concrete, the total deformation can be divided into the elastic deformation and the plastic deformation based on the classical elasto-plastic theory

$$\varepsilon = \varepsilon_e + \varepsilon_p \quad (3)$$

where ε , ε_e , and ε_p are total deformation, elastic deformation, and plastic deformation, respectively.

According to the iso-thermal, if the elastic strain is independent of strain hardening, then the Helmholtz free potential energy Ψ can be expressed by the following formula

$$\Psi(\varepsilon, D_0) = \psi_e(\varepsilon_e, D_0) + \psi_p(\eta, \varepsilon_p) \quad (4)$$

where ψ_e is elastic part of the Helmholtz free potential energy, ψ_p is plastic part of the Helmholtz free potential energy, D_0 is the internal variable of damage, η is the internal variable of ductility.

In the above formula, ψ_e can be expanded by the following formula

$$\psi_e(\varepsilon_e, D_0) = \frac{1}{2}(1 - D_0)E\varepsilon_e^2 \quad (5)$$

According to the second law of thermodynamics, the damage evolution and plastic deformation accumulation in concrete are irreversible. So the following Clausius-Duheim inequality can be satisfied

$$\sigma\varepsilon - \dot{\Psi} \geq 0 \quad (6)$$

According to the Eqs. (3), (5) and (6), the following formula can be derived

$$\sigma = \frac{\partial \Psi_e}{\partial \varepsilon_e} = (1 - D_0)E(\varepsilon - \varepsilon_p) \quad (7)$$

Thus, the Eq. (7) is elasto-plastic damage constitutive model. When D_0 equal to 0, the plastic deformation follows the law of plastic mechanics and the constitutive model above is converted into the linear elastic model. When ε_p equal to 0, the Eq. (7) can be converted into the following formula

$$\sigma = (1 - D_0)E\varepsilon \quad (8)$$

The above equation is the classical damage model (Mazars and Pijaudier-Cabot 1989). The damage generated by exterior load is defined as D_1 , the rate of micro-unit damage $\dot{\phi}$ can be written as the following formula

$$\frac{dD_1}{d\varepsilon} = \phi(\varepsilon) \quad (9)$$

Here Weibull model is used to describe the damage evolution of concrete

$$\phi(\varepsilon) = \frac{m}{\alpha^m} \left(\frac{\varepsilon - \gamma}{\alpha} \right)^{m-1} \exp \left[- \left(\frac{\varepsilon - \gamma}{\alpha} \right)^m \right] \quad (10)$$

where α , γ and m are the scale parameter, location parameter and shape parameter, respectively.

The following formula can be obtained by integrating the Eq. (9)

$$D_1 = 1 - \exp \left[- \left(\frac{\varepsilon - \gamma}{\alpha} \right)^m \right] \quad (11)$$

Here, Eq. (9) needs to satisfy the following four boundary conditions: (1) $\varepsilon=0$, $\sigma=0$; (2) $\varepsilon=0$, $\frac{d\sigma}{d\varepsilon} = E$; (3)

$\varepsilon=\varepsilon_c$, $\sigma=\sigma_c$; (4) $\varepsilon=\varepsilon_c$, $\frac{d\sigma}{d\varepsilon} = 0$, where ε_c is the peak strain

and σ_c is peak stress.

Following Eq. (12) can be obtained after differential of Eq. (8)

$$d\sigma = d[(1 - D_1)E\varepsilon] = Ed \left\{ \exp \left[- \left(\frac{\varepsilon - \gamma}{\alpha} \right)^m \right] \varepsilon \right\} \quad (12)$$

Thus

$$\frac{d\sigma}{d\varepsilon} = E \left\{ - \frac{m\varepsilon}{\alpha} \left(\frac{\varepsilon - \gamma}{\alpha} \right)^{m-1} \exp \left[- \left(\frac{\varepsilon - \gamma}{\alpha} \right)^m \right] + \exp \left[- \left(\frac{\varepsilon - \gamma}{\alpha} \right)^m \right] \right\} \quad (13)$$

The boundary condition (3) is substituted in Eqs. (8) and (11), then

$$\ln \frac{E}{E'} = \left(\frac{\varepsilon_c - \gamma}{\alpha} \right)^m \quad (14)$$

where E' is peak secant modulus. The value equals to σ_c/ε_c .

So the scale parameter expression can be obtained

$$\alpha = \frac{\varepsilon_c - \gamma}{\left[\ln \left(\frac{E}{E'} \right) \right]^{\frac{1}{m}}} \quad (15)$$

The boundary condition (4) is substituted in Eq. (13), Eq. (16) can be obtained as following

$$E \left\{ - \frac{m\varepsilon_c}{\alpha} \left(\frac{\varepsilon_c - \gamma}{\alpha} \right)^{m-1} \exp \left[- \left(\frac{\varepsilon_c - \gamma}{\alpha} \right)^m \right] + \exp \left[- \left(\frac{\varepsilon_c - \gamma}{\alpha} \right)^m \right] \right\} = 0 \quad (16)$$

The positions of terms are changed, then the Eq. (17) can be got as following

$$\frac{m\varepsilon}{\alpha} \left(\frac{\varepsilon - \gamma}{\alpha} \right)^{m-1} \exp \left[- \left(\frac{\varepsilon - \gamma}{\alpha} \right)^m \right] = \exp \left[- \left(\frac{\varepsilon - \gamma}{\alpha} \right)^m \right] \quad (17)$$

Both sides of Eq. (17) are divided by the non-zero term

$$\exp \left[- \left(\frac{\varepsilon - \gamma}{\alpha} \right)^m \right] : \frac{m\varepsilon}{\alpha} \left(\frac{\varepsilon - \gamma}{\alpha} \right)^{m-1} = 1 \quad (18)$$

Eq. (14) is substituted in Eq. (18)

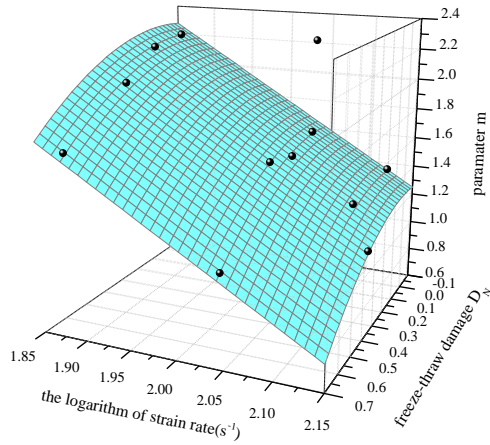


Fig. 6 The relationship between the parameter m , strain rate and the freeze-thaw damage

$$\frac{m\varepsilon_c \ln \frac{E}{E'}}{\alpha} = \frac{\varepsilon_c - \gamma}{\alpha} \quad (19)$$

Then the shape parameter expression can be obtained

$$m = \frac{\varepsilon_c - \gamma}{\varepsilon_c \ln \frac{E}{E'}} \quad (20)$$

Thus, according to Eqs. (8), (11), (15) and (20), the dynamic damage constitutive model for concrete after freeze-thaw cycles can be expressed by the following equation

$$\begin{aligned} \sigma &= E\varepsilon(1 - D_1) = E\varepsilon \exp \left[- \left(\frac{\varepsilon - \gamma}{\alpha} \right)^m \right] \\ &= E\varepsilon \exp \left[- \frac{\varepsilon_c - \gamma}{\varepsilon_c m} \left(\frac{\varepsilon - \gamma}{\varepsilon_c - \gamma} \right)^m \right] \end{aligned} \quad (21)$$

In this test, the split Hopkinson pressure bar was used to generate the impact load and the strain gauges on the specimen were used to determine the strain of concrete specimen. When the impact load on the specimen reached the strength of concrete, the specimen was failure and strain gauges were also destroyed. Therefore, only the ascending branch of stress-strain curve was obtained.

In the ascending branch, the following conditions are satisfied: $\varepsilon \leq \varepsilon_c$ and $\gamma=0$ (Wang *et al.* 2008). So Eq. (21) can be simplified as following

$$\sigma = E\varepsilon \exp \left[- \frac{1}{m} \left(\frac{\varepsilon}{\varepsilon_c} \right)^m \right] \quad (22)$$

where the value of m is related with strain rate $\dot{\varepsilon}$ and freezing-thawing damage D_N , as shown in Fig. 6. This relation can be formally written as

$$m = 8.625 - 0.9941D_N^2 - 3.426\log(\dot{\varepsilon}), \quad R^2 = 0.89 \quad (23)$$

The comparison of predicted and experimental results is shown in Fig. 5. Fig. 7 shows the relationship among peak stress, strain rate and the number of freeze-thaw cycles. Fig.

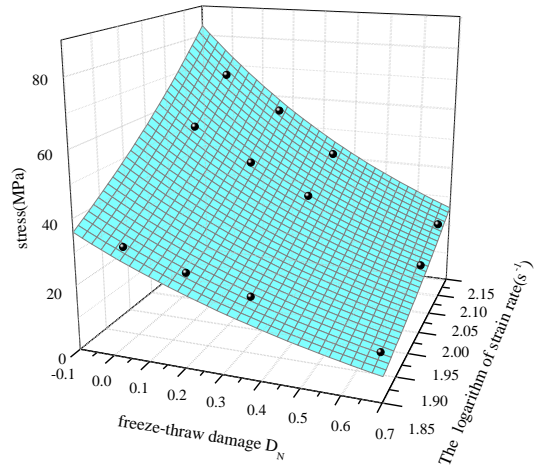


Fig. 7 The relationship between peak stress, strain rate and the freeze-thaw damage

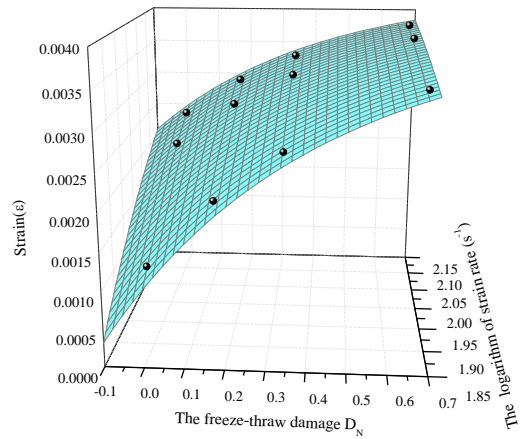


Fig. 8 The relationship between peak strain, strain rate and the freeze-thaw damage

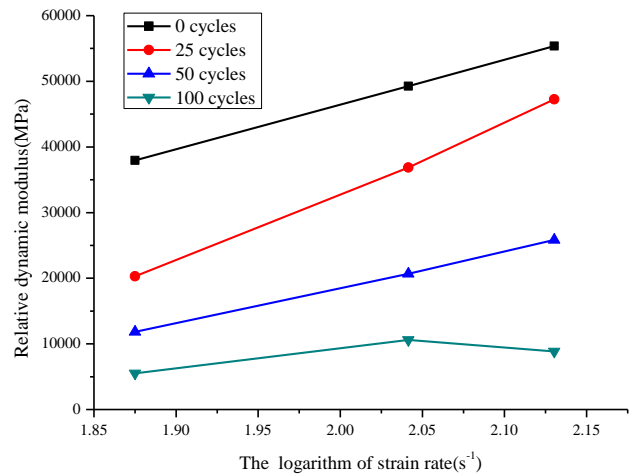


Fig. 9 The relationship between RDM, strain rate and the freeze-thaw cycles

8 shows the relationship among peak strain, strain rate and the number of freeze-thaw cycles. Fig. 9 shows the relationship among elastic modulus, strain rate and the freeze-thaw cycles.

4. Fractal characteristics of concrete under high strain rates

Fractal refers to the self-correlation shown by matters (Issa *et al.* 2003). For example, the local and the whole of the matter are similar, and there will be a fractal dimension. Fractal initially was used to study math problems and later extended to various areas (Pia and Sanna 2013). Most of the fractal things in nature are self-affine and random. Although they are not self-similar absolutely, they are similar statistically. For now, the fractal is also widely used in the research field of microstructure and macro mechanical properties of concrete (Yang and Wang 2015, Jin *et al.* 2013, Hu *et al.* 2015). In this paper, concrete fragments from each test were collected and screened through sieves with 0.075 mm, 0.15 mm, 0.3 mm, 0.6 mm, 1.2 mm, 2.5 mm, 5.0 mm and 10.0 mm aperture. Then each group fragments were weighed. There are two very typical distributions on the study of fragments, which are R-R (Rosin-Rammler) distribution and G-G-S (Gate-Gaudin-Schuhmann) distribution. The formula of R-R distribution is written as following (Zhou *et al.* 2006)

$$y = 1 - \exp[-(r/r_0)^\alpha] \quad (24)$$

where r_0 is feature size and α is distributed parameter.

The formula of G-G-S distribution is written as following

$$y = (r/r_m)^b \quad (25)$$

where r_m is the maximum size and b is a regression coefficient.

If high order terms are ignored, the same calculation result can be got, by comparing Eqs. (24) and (25), thus

$$\frac{m(r)}{M} = \left(\frac{r}{r_m}\right)^b \quad (26)$$

where, $m(r)$ is the percentage of fragments through the aperture r , M is the total weight of fragments.

According to Eq. (26), the following can be obtained

$$dm \propto r^{b-1} dr \quad (27)$$

The following formula can be obtained by the relation between slag diameter and weight

$$dm \propto r^3 dN \quad (28)$$

The following formula can be obtained according to the definition of fractal

$$D = \frac{\ln N(F)}{\ln r} \quad (29)$$

where r is diameter, F is slag, N is the times of slag determined by r . Thus

$$N \propto r^{-D} \quad (30)$$

$$dN \propto r^{-D-1} dr \quad (31)$$

Through Eqs. (27)-(31)

$$D = 3 - b \quad (32)$$

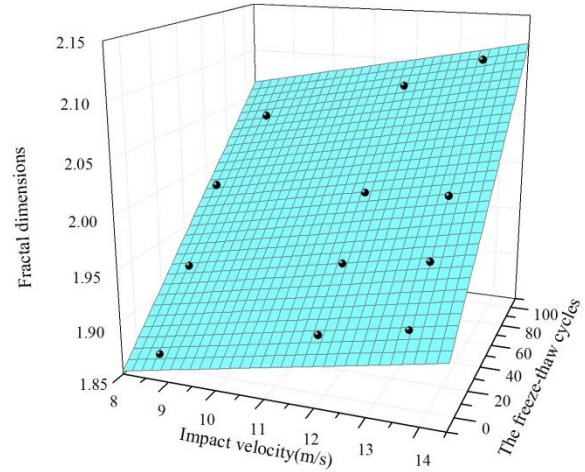


Fig. 10 The relationship between the fractal dimensions, impact velocity and freeze-thaw cycles

So the effect of impact velocity and number of freeze-thaw cycles on fractal dimension of concrete slag can be obtained, as shown in Fig. 10. It can be found that fractal dimension increases with the increasing of freeze-thaw cycles and impact velocity.

5. Conclusions

In this paper, dynamic compression tests on concrete specimens after various freeze-thaw cycles were conducted by using the split Hopkinson pressure bar (SHPB). The following conclusions can be drawn according to analysis of experimental results:

- With the increase of freeze-thaw cycles the weight loss ratio and the loss ratio of the relative dynamic elastic modulus are increased. When the number of freeze-thaw cycles is less than 50, the mass loss of concrete increases slightly with the increasing of freeze-thaw cycles. When the freeze-thaw cycles are in the range of 50 to 100, the growth of the mass loss is small and the mass loss versus cycles curve is more stable.
- The rate-sensitivity of concrete after freezing and thawing is obvious. The dynamic compressive strength of concrete increases with the strain rate. The dynamic strength decreases and the peak strain increases with the increasing of freeze-thaw cycles.
- Based on the Weibull distribution model, statistical damage constitutive model for dynamic stress-strain response of concrete after freeze-thaw cycles was proposed. This model can well predict the stress and strain of concrete under high strain rates. The shape parameter decreases with the increasing of freeze-thaw cycles and strain rate.
- The fractal dimension of concrete fragments under different impact velocities and various freeze-thaw cycles was obtained. The fractal dimensions of concrete increase with the increasing of both freeze-thaw cycle and strain rate.

Acknowledgements

This research is based upon work support supported by the National Key R&D Program of China (SN: 2016YFC0401907); National Natural Science Foundation of China (SN: 51679150, 51409162 and 51579153) and the Fund Project of NHRI (Y417001; Y417015).

References

- Aitcin, P.C. (2003), "The durability characteristics of high performance concrete: a review", *Cement Concrete Compos.*, **25**(4-5), 409-420.
- ASTM C215 (2014), Standard Test Method for Fundamental Transverse, Longitudinal, and Torsional Resonant Frequencies of Concrete Specimens, ASTM International, West Conshohocken, PA, USA.
- ASTM C666 (2015), Standard Test Method for Resistance of Concrete to Rapid Freezing and Thawing, ASTM International, West Conshohocken, PA, USA.
- Chen, F. and Qiao, P. (2015), "Probabilistic damage modeling and service-life prediction of concrete under freeze-thaw action", *Mater. Struct.*, **48**(8), 2697-2711.
- Chen, J.J., Guo, B.Q., Liu, H.B., Liu, H. and Chen, P.W. (2014), "Dynamic Brazilian test of brittle materials using the split Hopkinson pressure bar and digital image correlation", *Strain*, **50**(6), 563-570.
- Chen, X., Wu, S. and Zhou, J. (2013), "Experimental and modeling study of dynamic mechanical properties of cement paste, mortar and concrete", *Constr. Build. Mater.*, **47**(10), 419-430.
- Chen, X., Wu, S. and Zhou, J. (2014), "Experimental study on dynamic tensile strength of cement mortar using split hopkinson pressure bar technique", *J. Mater. Civil Eng.*, ASCE, **26**(6), 150-153.
- Chen, X., Xu, L. and Wu, S. (2015), "Influence of pore structure on mechanical behavior of concrete under high strain rates", *J. Mater. Civil Eng.*, ASCE, **28**(2), 04015110.
- Choi, W.C. and Yun, H.D. (2014), "Acoustic emission activity of CFRP-strengthened reinforced concrete beams after freeze-thaw cycling", *Cold Reg. Sci. Tech.*, **110**, 47-58.
- Daghash, S.M., Soliman, E.M., Kandil, U.F. and Taha, M.M.R. (2016), "Improving impact resistance of polymer concrete using CNTs", *Int. J. Concrete Struct. Mater.*, **10**(4), 1-15.
- Hu, J., Qian, Z., Wang, D. and Oeser, M. (2015), "Influence of aggregate particles on mastic and air-voids in asphalt concrete", *Constr. Build. Mater.*, **93**, 1-9.
- Issa, M.A., Islam, M.S. and Chudnovsky, A. (2003), "Fractal dimension-a measure of fracture roughness and toughness of concrete", *Eng. Fract. Mech.*, **70**(1), 125-137.
- Jiang, L., Niu, D., Yuan, L. and Fei, Q. (2014) "Durability of concrete under sulfate attack exposed to freeze-thaw cycles", *Cold Reg. Sci. Tech.*, **112**, 112-117.
- Jin, S., Zhang, J. and Huang, B. (2013), "Fractal analysis of effect of air void on freeze-thaw resistance of concrete", *Constr. Build. Mater.*, **47**(5), 126-130.
- Lai, Y., Guo, H. and Dong, Y. (2009), "Laboratory investigation on the cooling effect of the embankment with l-shaped thermosyphon and crushed-rock revetment in permafrost regions", *Cold Reg. Sci. Tech.*, **58**(3), 143-150.
- Lai, Y., Li, S., Qi, J., Gao, Z. and Chang, X. (2008), "Strength distributions of warm frozen clay and its stochastic damage constitutive model", *Cold Reg. Sci. Tech.*, **53**(2), 200-215.
- Li, W., Luo, Z., Long, C. and Shah, S.P. (2016), "Effects of nanoparticle on the dynamic behaviors of recycled aggregate concrete under impact loading", *Mater. Des.*, **112**, 58-66.
- Li, W., Luo, Z., Wu, C. and Shah, S.P. (2017), "Experimental and numerical studies on impact behaviors of recycled aggregate concrete-filled steel tube after exposure to elevated temperature", *Mater. Des.*, **136**, 103-118.
- Li, W., Pour-Ghaz, M., Castro, J. and Weiss, J. (2012), "Water absorption and critical degree of saturation relating to freeze-thaw damage in concrete pavement joints", *J. Mater. Civil Eng.*, ASCE, **24**(3), 299-307.
- Lim, K.M., Shin, H.O., Kim, D.J., Yoon, Y.S. and Lee, J.H. (2016), "Numerical assessment of reinforcing details in beam-column joints on blast resistance", *Int. J. Concrete Struct. Mater.*, **10**(s3), 1-10.
- Liu, M.H. and Wang, Y.F. (2012), "Damage constitutive model of fly ash concrete under freeze-thaw cycles", *ASCE J. Mater. Civil Eng.*, **24**(9), 1165-1174.
- Lu, H., Peterson, K. and Chernoloz, O. (2016), "Measurement of entrained air-void parameters in portland cement concrete using micro x-ray computed tomography", *Int. J. Pavement Eng.*, **6**, 1-13.
- Mazars, J. and Pijaudier-Cabot, G. (1989), "Continuum damage theory-application to concrete", *J. Eng. Mech.*, ASCE, **115**(2), 345-365.
- Ozbolt, J., Sharma, A., İrhan, B. and Sola, E. (2014), "Tensile behavior of concrete under high loading rates", *Int. J. Impact Eng.*, **69**, 55-68.
- Pia, G., and Sanna, U. (2013), "A geometrical fractal model for the porosity and thermal conductivity of insulating concrete", *Constr. Build. Mater.*, **44**, 551-556.
- Richard, B., Quiertant, M., Bouteiller, V., Delaplace, A., Ragueneau, F. and Cremona, C. (2016). Experimental and numerical analysis of corrosion-induced cover cracking in reinforced concrete sample", *Comput Concrete*, **18**(3), 421-439.
- Richardson, D.N. and Lusher, S.M. (2015), "Prediction of freezing-and-thawing durability of concrete", *ACI Mater. J.*, **112**(3), 439-450.
- Safiuddin, M., Gonzalez, M., Cao, J. and Tighe, S.L. (2014), "State-of-the-art report on use of nano-materials in concrete", *Int. J. Pavement Eng.*, **15**(10), 940-949.
- Shang, H.S., Zhao, T.J. and Cao, W.Q. (2015), "Bond behavior between steel bar and recycled aggregate concrete after freeze-thaw cycles", *Cold Reg. Sci. Tech.*, **118**, 38-44.
- Sun, W., Mu, R., Luo, X. and Miao, C. (2002), "Effect of chloride salt, freeze-thaw cycling and externally applied load on the performance of the concrete", *Cement Concrete Res.*, **32**(12), 1859-1864.
- Sun, W., Zhang, Y.M., Yan, H.D. and Mu, R. (1999), "Damage and damage resistance of high strength concrete under the action of load and freeze-thaw cycles", *Cement Concrete Res.*, **29**(9), 1519-1523.
- Tanyildizi, H. (2017), "Prediction of compressive strength of lightweight mortar exposed to sulfate attack", *Comput Concrete*, **19**(2), 217-226.
- Tian, Z., Bu, J., Bian, C. and Peng, Z. (2016), "Effect of strain rate and saturation on uniaxial dynamic compressive behaviours of mortar", *Int. J. Pavement Eng.*, **17**(9), 789-798.
- Wang, Z.L., Liu, Y.S. and Shen, R.F. (2008), "Stress-strain relationship of steel fiber-reinforced concrete under dynamic compression", *Constr. Build. Mater.*, **22**(5), 811-819.
- Xiao, J., Li, L., Shen, L. and Chi, S.P. (2015), "Compressive behaviour of recycled aggregate concrete under impact loading", *Cement Concrete Compos.*, **71**, 46-55.
- Yang, X. and Wang, F. (2015), "Random-fractal-method-based generation of meso-model for concrete aggregates", *Powder Tech.*, **284**(14), 63-77.
- Yun, Y. and Wu, Y.F. (2011), "Durability of CFRP-concrete joints under freeze-thaw cycling", *Cold Reg. Sci. Tech.*, **65**(3), 401-

412.

- Zhang, X.X., Elazim, A.M.A., Ruiz, G. and Yu, R.C. (2014), "Fracture behaviour of steel fibre-reinforced concrete at a wide range of loading rates", *Int. J. Impact Eng.*, **71**(6), 89-96.
- Zhou, Z., Li, X., Zuo, Y. and Hong, L. (2006), "Fractal characteristics of rock fragmentation at strain rate of 10^0 - 10^2 s⁻¹", *J. Central South Univ. Technol., Mater. Sci. Edi.*, **13**(3), 290-294.

AW